Statistical Characteristics of Thin, Wavy Films

III. Structure of the Large Waves and their Resistance to Gas Flow

Two classes of random waves exist on falling films at flow rates of practical interest; large waves which carry the bulk of the liquid and small waves which cover the substrate. In this paper statistics of the large waves are presented and compared with existing theory. These waves are bimodal in character at $Re_L > 700$. The form drag of the large waves is shown to contribute negligibly the observed pressure drop in the gas phase. It is thus concluded that the small wave structure controls the fluid resistance and transfer processes in the gas while the large waves control these same processes in the liquid film.

K. J. CHU

and

A. E. DUKLER

Chemical Engineering Department
University of Houston
Houston, Texas 77004

SCOPE

The uses of thin liquid films in modern process technology are numerous and important. These include trickling-type cooling towers, packed and wetted-wall towers for rectification and gas absorption, gas-liquid pipeline chemical reactors and various types of reboilers, coolers, and evaporators, (Guerreri and King, 1974; Sack, 1967). The gas-liquid interface of these films is usually covered by waves. It has already been shown (Telles and Dukler, 1970) that two types of random waves exist at the interface. One class consists of large lumps of liquid which carry a significant portion of all flowing liquid. These move down the interface with essentially constant speed, different lumps or waves having randomly distributed amplitude and shape. The other is a smaller wave structure which exists over the substrate as well as across the large waves. This class too has certain random features. The rates of transfer of momentum, heat, and mass are greatly enhanced by the presence of these random waves (Dukler, 1972) because the waves modify the velocity distribution of the film as well as in the gas phase and makes them time dependent. Most design procedures for heat and mass transfer assume a smooth interface and, as a result, these design methods have been inaccurate (Cichy et al., 1969; Alves, 1970).

The approach toward developing improved designs requires first that accurate information be available on the wave structure and how it varies with flow conditions. Then the observed wave structure must be related to the new distributions of velocities which exist. Knowing the new velocities, it is possible to attempt to solve the diffusion equation for heat and mass transfer. In an earlier paper, Chu and Dukler (1974) described methods for extracting the statistics of the wave motion from a time series analysis of the film thickness. There the small wave structure was treated. In this paper the large waves which control the liquid film flow are analyzed for a wide range of conditions of liquid flow rate and concurrent gas flows which impose interfacial shear. The objective is also to determine the degree to which these large waves influence pressure drop and transfer in the gas phase. In a future paper a model relating the observed wave structure to the velocity distributions will be presented.

CONCLUSIONS AND SIGNIFICANCE

The structure of the large waves is examined in detail. Above a liquid Reynolds number of about 700 these waves are shown to be bimodal in character (Figures 9, 10, and 17). At all flow conditions, they are highly asymmetric in shape (Figure 14) and of low frequency (Figure 15). A method of extracting the form drag of these waves from the cross correlation between film thickness and pressure is demonstrated. From these measurements it is shown that the large waves contribute little to the very large pressure drops observed in the gas flowing over the wavy interface. It is thus concluded that the large wave structure controls the hydrodynamic behavior of the liquid film and the associated transfer process. However, the small waves on the substrate control the processes of transfer in the gas phase.

Comparison of the statistics of the large waves with existing theories for wave amplitude, length, frequency, and velocity show very poor agreement. This is attributed to the fact that all such theories have used only a few terms in a Fourier series to model the wave shape. With the data collected here, it is evident that many more Fourier terms would be required than could be practically accommodated. Thus alternate approaches are necessary based on different orthogonal expansions which can, in fewer terms, describe the actual shapes that exist. Such a procedure is to be described in the next paper.

Correspondence concerning this paper should be addressed to A. E. Dukler. K. J. Chu is with C. F. Braun Company, 1000 S. Fremont, Alhambra, California 91802.

Measurements treating the film thickness as a random process are relatively recent developments. Limited studies by Wicks (1967), Telles (1968), Pashniak (1969), and Webb (1970) have been made to obtain such measurements. In all of these reports, the randomness of the interface was represented by the probability distribution or the spectral density of the film thickness, but there was no attempt to extract the needed information about the structure of the waves. Typical film thickness traces showing the presence of waves on falling films are shown in Figure 1. Telles and Dukler (1970) in the first paper of this series showed that the gas-liquid interface consists of a two wave structure and made an initial attempt to extract information on the structure of the large waves from the film thickness measurements. Chu and Dukler (1974) in the second paper reported in detail on the statistical character of the substrate and its small waves.

The purpose of this paper is to present new information on the structure of the large waves. A future paper will consider a theoretical model for the large waves on liquid films. Two groups of statistical parameters are used here: One considers the film thickness itself as a random process and another considers individual large waves as a random process. Detailed data are presented by Chu (1973).

EXPERIMENTAL EQUIPMENT

The flow system consisted of a 4.27-m long vertical test section with four measuring stations, a 1.72-m long air-water entry section and a 0.61-m long air-water separation section. A schematic flow diagram of the apparatus is given in Figure 2. The test section was made of 4 lengths of 5.080 ± 0.005-cm I.D. Plexiglass pipe with lengths of 0.305 m, 0.610 m, 1.220 m, and 1.830 m. There were four measuring stations located between these lengths of test section. Each individual station consisted of four pairs of conductivity probes located at 90° intervals around the circumference for film thickness measurement and four pressure channels to measure instantaneous pressure. The equipment, electronic circuity, calibration procedure, and data processing scheme for film thickness is treated in detail by Chu and Dukler (1974). Instantaneous pressure was measured by connecting a short liquid filled line from the pressure tap in the measuring station to a DISA PU2A pressure transducer of the capacitance type. The connecting line was designed to ensure that the resonant frequency of this cavity did not overlap the frequency range of interest. The accuracy of the time series $h(t)$ is estimated to be 0.025 mm in the amplitude domain and 0.004 s in the time domain. For the time series $p(t)$, the amplitude accuracy is estimated to be 0.7-mm water.

The data reported here were taken at a location 4.17 m down from the inlet.

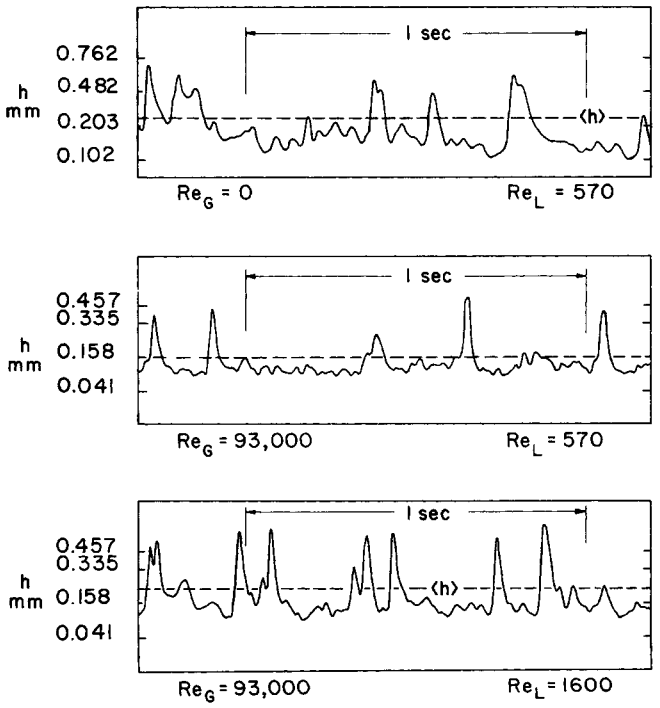

Fig. 1. Typical film thickness traces.

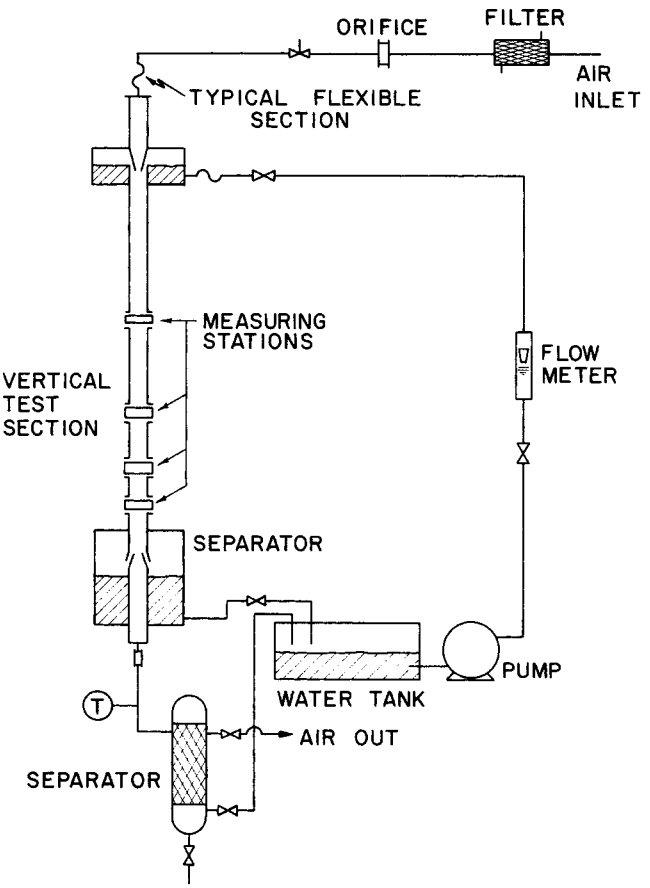

Fig. 2. Schematic of experimental equipment.

STATISTICAL DATA ANALYSIS

Large Waves

Methods for discriminating between small and large waves have been discussed by Chu and Dukler (1974). In order to characterize the random large wave it is necessary to calculate the mean value, variance, and probability density function of seven wave parameters which are identified in Figure 3. The procedure for data processing to accomplish this purpose is also given by Chu and Dukler (1974). In the time domain, the wave parameters of interest are: time for passage of the base, T_b, wave separation time T_s, time for passage of the wave front T_{bf}, and time for passage of the back of the wave T_{bb}. Note that separation time T_s differs from the base dimension T_b because of the existence of a wavy substrate between two successive large waves. In the amplitude domain, the wave parameters of interest are amplitude A, film thickness at the maximum of the wave h_{mx}, and film thickness at the minimum of the wave h_{mn}. Because the minimum film thickness in front and in back of wave are not usually equal, the definition of wave amplitude used is

$$2A = h_{mx} - (h_{mn} + h'_{mn})/2 \qquad (1)$$

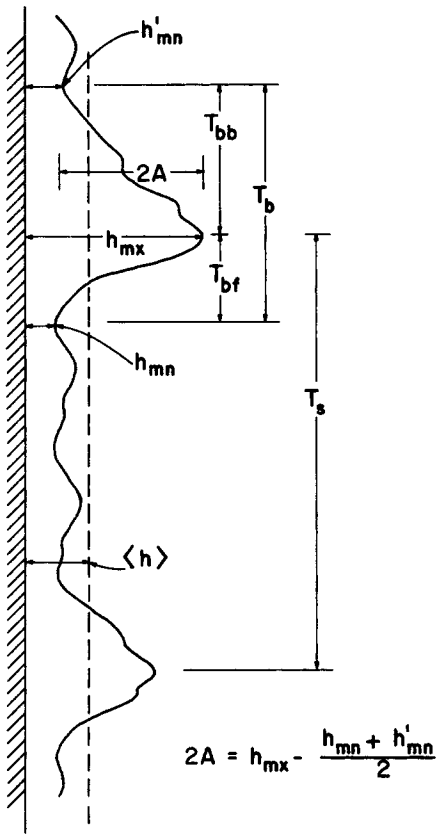

Fig. 3. Large wave parameters.

The Film Thickness $\hat{h}(t)$ and Pressure $\hat{p}(t)$

Since the instantaneous film thickness $\hat{h}(t)$ is a random fluctuating quantity, time series analysis can be used to provide statistical parameters such as the mean film thickness $<h>$, central moments $\tilde{\mu}_i$, probability density function $\tilde{f}(h)$, spectral density $\tilde{S}_{ij}(f)$, and covariance function $\tilde{C}_{ij}(\tau)$. These are defined in the following equations under the assumption of stationarity and ergodicity of this stochastic process:

$$\tilde{F}_h(h) = \text{Prob}\,\{\hat{h}(t) \leq h\} \tag{2}$$

$$\tilde{f}_h(h) = d\tilde{F}_h(h)/dh \tag{3}$$

$$<h(t)> = \int_{-\infty}^{+\infty} h\,\tilde{f}_h(h)\,dh \tag{4}$$

$$\tilde{\mu}_i = \int_{-\infty}^{+\infty} (h - <h>)^i \tilde{f}_h(h)\,dh \quad i \geq 2 \tag{5}$$

$$\tilde{C}_{ij}(\tau) = <(h_i(t+\tau) - <h_i>)\,(h_j(t) - <h_j>)> \tag{6}$$

$$\tilde{S}_{ij}(f) = \int_{-\infty}^{+\infty} e^{-i2\pi f\tau}\,C_{ij}(\tau)\,d\tau \tag{7}$$

where $\hat{h}_i(t)$ is the film thickness time series measured at the ith station. Spectra and covariance function were calculated using fast Fourier transform processing of digitized data. Among the above statistical parameters, directly measured probability density function and covariance functions of the film thickness have never before been reported. Similar analysis was done on the wall pressure trace $\hat{p}(t)$. This is the first such data to be reported.

EXPERIMENTAL RESULTS

Film Thickness $\hat{h}(t)$

Probability Density function for the film thickness, $\tilde{f}(h)$.

Directly measured values of $\tilde{f}(h)$ for five liquid rates at zero gas flow appear in Figure 4 and for three gas rates at one liquid rate are shown in Figure 5. The following general characteristics are observed:

1. The curve is highly asymmetrical around the modal value.
2. The maximum peak values decrease sharply with increasing liquid and gas rate.
3. A long tail exists which stretches to over 6 times the modal value.

These observations show that there exists a substrate film corresponding to the modal value of the curve along with many large waves which ride on the substrate film and which have a range of wave amplitudes. The characteristics of the modal peak and its interpretation in terms of the substrate have already been analyzed by Chu and Dukler (1974).

The existence of these directly measured probability densities makes it possible to make accurate determinations of the moments. Such calculations (Chu, 1973) confirm, in general, certain statistical characteristics of the large waves as suggested by Telles and Dukler (1970) from much cruder measurements, namely,

1. The normalized third central moment is substantial in magnitude compared to the second moment for all flow

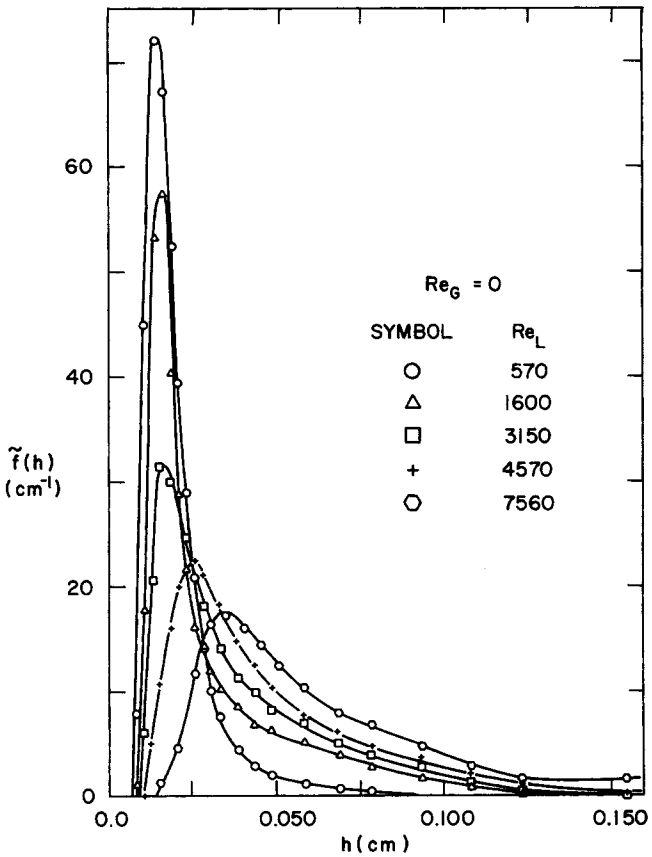

Fig. 4. Probability density of film thickness. $Re_G = 0$: varying liquid rates.

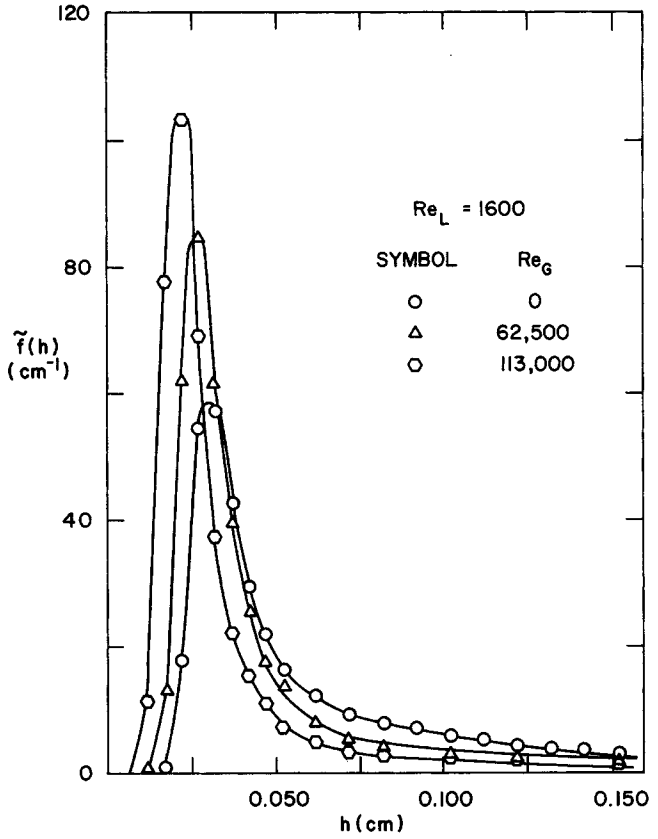

Fig. 5. Probability density of film thickness. $Re_L = 1600$: varying gas rates.

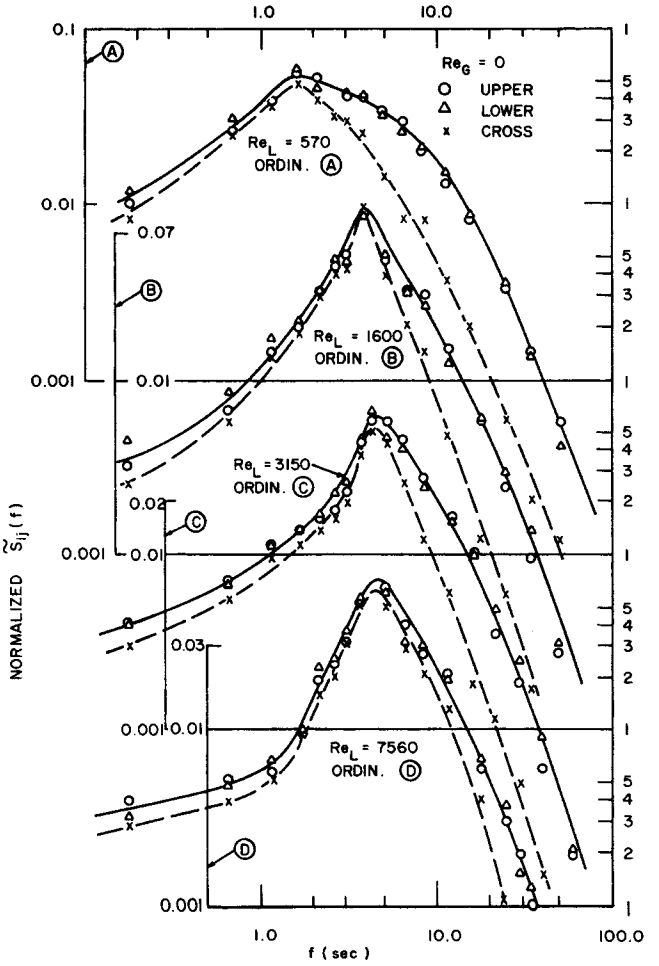

Fig. 6. Spectral density of film thickness. $Re_G = 0$: varying liquid rates.

conditions, thus Gaussian density distributions, often used in the past, do not describe the stochastic process of film thickness.

2. The standard deviation is of the same order of magnitude as the mean. Thus, mathematical models based on the idea that wave amplitude is small compared to the mean film thickness are open to question.

Spectral Density of the Film Thickness. Seven typical film thickness spectral densities at various liquid and gas flow rates are shown in Figure 6 and 7. Also shown are the cross spectra of the film thickness taken at stations separated by 30.5 cm in the vertical direction. All the spectral data are normalized by the second central moment of the film thickness, and the cross spectra are normalized by the square root of the product of the two second central moments measured at the two probes. Under all conditions, the spectral densities display a well defined maximum designated as the frequency f_m. This modal frequency increases slightly with gas and liquid rates. In all cases, f_m is below 10 cycles per second and is thus characteristic of the large waves.

The cross amplitude spectrum at low frequencies is almost identical with the two auto spectral densities. As the frequency increases, the cross amplitude spectrum increasingly departs from the auto spectra especially for the lower liquid rates. This change suggests that the high frequency small waves do not maintain their identity over the short separation distance between probes. On the other hand, the low frequency waves move with little or no change in size or shape.

The shape of these spectra are qualitatively similar to those of ocean waves although for ocean waves modal frequency is considerably lower and the spread of frequency is less. Phillips (1958) has shown that the higher frequency end of the water wave spectrum can be ex-

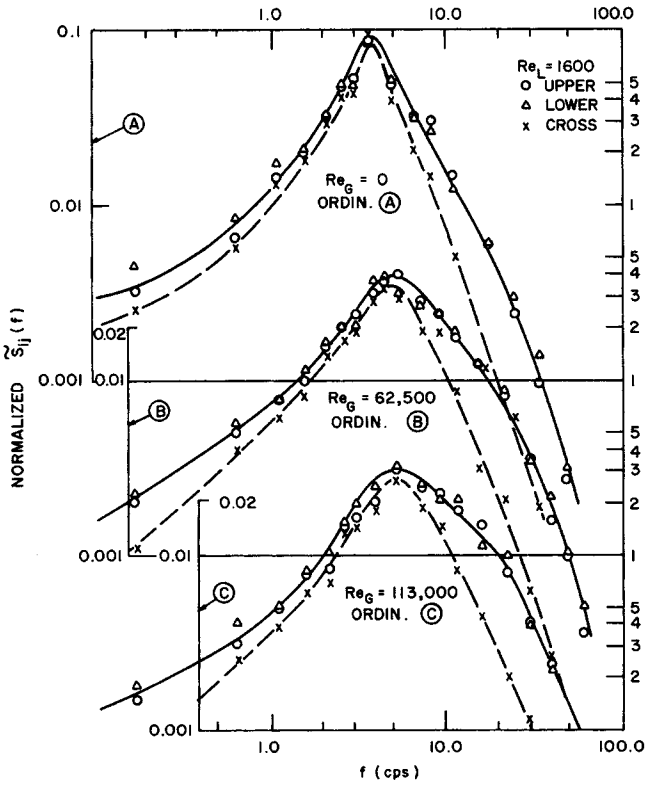

Fig. 7. Spectral density of film thickness. $Re_L = 1600$: varying gas rates.

Table 1. Slope of Film Thickness Spectra in the Equilibrium Range

Re_G / Re_L	0	29,000	62,500	91,900	113,500
211	−2.94	−3.89	−4.28	−3.89	—
388	−2.93	−3.60	−3.90	−4.00	−3.67
565	−2.77	−3.42	−3.30	−3.67	−3.74
986	−2.85	−3.36	−3.86	−3.73	−3.63
1,558	−2.86	−3.48	−3.62	−3.63	−3.67
2,140	−2.85	−3.69	−3.62	−3.89	−3.62
2,850	−2.84	−3.60	−3.80	−3.89	−3.77
4,110	−2.85	−3.69	−3.72	−3.65	−3.64
5,480	−2.85	−3.69	−3.52	−3.79	−3.64
6,790	−2.85	−3.69	−3.42	−3.72	−3.64

pected to vary as f^{-5}. His arguments which are germain to this study follow: The sea is covered by waves of all possible lengths shorter than some larger length which is in the state of breaking. Breaking occurs because local acceleration at the crest of the breaking wave exceeds the acceleration of gravity. This process controls wave shape and thus the spectrum at high frequencies. Phillips' approach is thus based on the idea that there exists a range of high frequencies determined entirely by gravity. By straightforward dimensional analysis he then arrives at

$$\tilde{S}_{eq}(f) = C_1 g^2 f^{-5} \tag{8}$$

Hess, Hidy, and Plate (1969) have obtained data in excellent agreement with this equation while data by Burling (1959) shows a −5.5 power dependence and Kinsman (1960) a −4.5 power law. On the whole, the validity of the minus 5th power law is well confirmed. However, the physical mechanism is still not fully clear because some wave spectral data have been obtained showing this dependence without the appearance of white caps which indicate the existence of breaking waves.

In a parallel analysis, Hicks (1963) has suggested that for capillary waves (in contrast to Phillips' gravity waves) the relationship should be

$$\tilde{S}_{eq}(f) = C_2 \gamma^{2/3} f^{-7/3} \tag{9}$$

where γ is the ratio of surface tension to density. Capillary waves are characterized by frequencies between 10-100 cps, much higher than usually observed on the sea. As a result, sea wave data can not be used to confirm Hicks hypothesis.

The existence of an equilibrium spectra for waves as falling films can be seen from the data in Table 1. Shown here is the measured slope of the spectral density curves at the higher frequencies (35 to 60 cps). The data fall into two groups whose slopes are remarkably constant over the full range of gas and liquid rates. In the absence of gas flow the equilibrium slope is −8/3. With gas flow and its accompanying interfacial shear, the slope of the spectrum at higher frequencies is remarkably uniform at −11/3 for all gas and liquid rates. These results fall between the prediction of Phillips (−15/3) and that of Hicks (−7/3), a situation to be expected since wave frequencies are such that both capillarity and gravity are important.

With these data it is possible to apply dimensional analysis to determine the surface tension and gravity dependence of the equilibrium spectra.

$$\tilde{S}_{eq}(f) = C_3 g^{1/4} \gamma^{7/12} f^{-8/3} \quad \text{(no gas flow)} \tag{10}$$

$$\tilde{S}_{eq}(f) = C_4 g \gamma^{1/3} f^{-11/3} \quad \text{(gas flow)} \tag{11}$$

Structure of the Large Waves

Experimental data for large wave parameters is shown here. Numerous theoretical studies have been proposed to predict the structure of waves on falling films. These have been reviewed by Dukler (1972). The large wave data obtained in this study enable one to make definitive tests of these theories. As will be shown, all are inadequate.

Wave Amplitude A. Probability density functions of wave amplitude $\tilde{f}_A(A)$ for a range of liquid rates in the absence of gas flow are shown in Figure 8. Except for the lowest flows, these density functions display well defined multiple peaks and thus suggest the existence of several discrete large wave sizes. At low liquid rates ($Re_L \leq 700$), the probability density is unimodal, indicating one characteristic wave amplitude with a modal

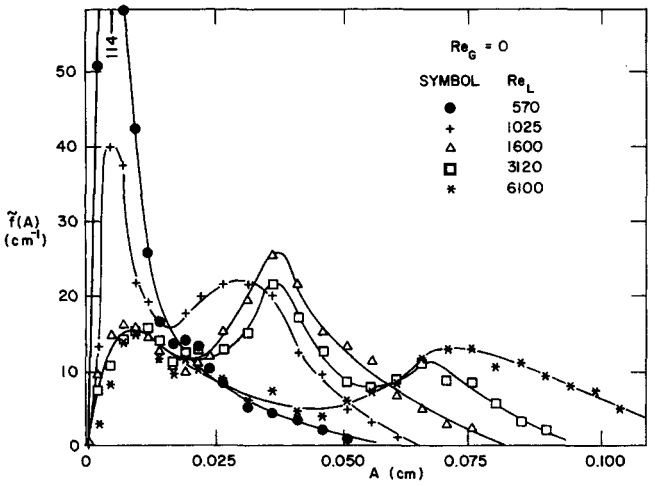

Fig. 8. Probability density of wave amplitude. $Re_G = 0$: varying liquid rates.

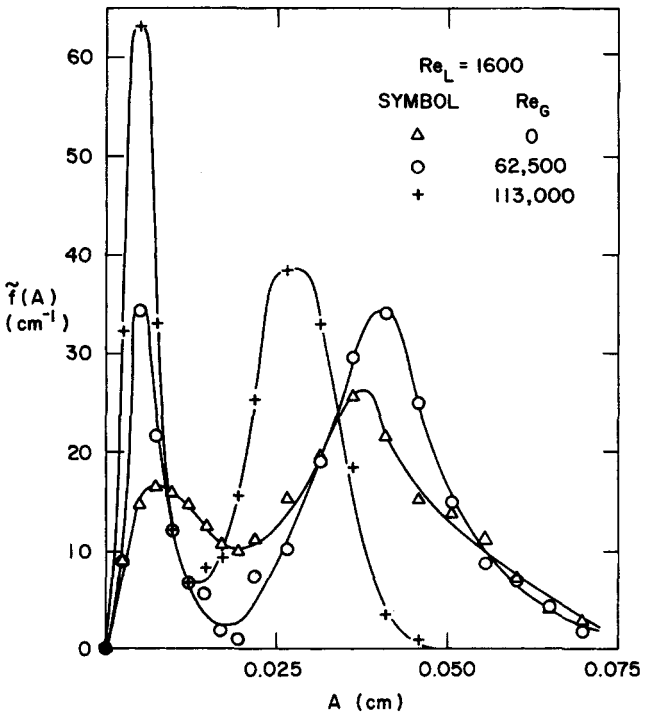

Fig. 9. Probability density of wave amplitude. $Re_L = 1600$: varying gas rates.

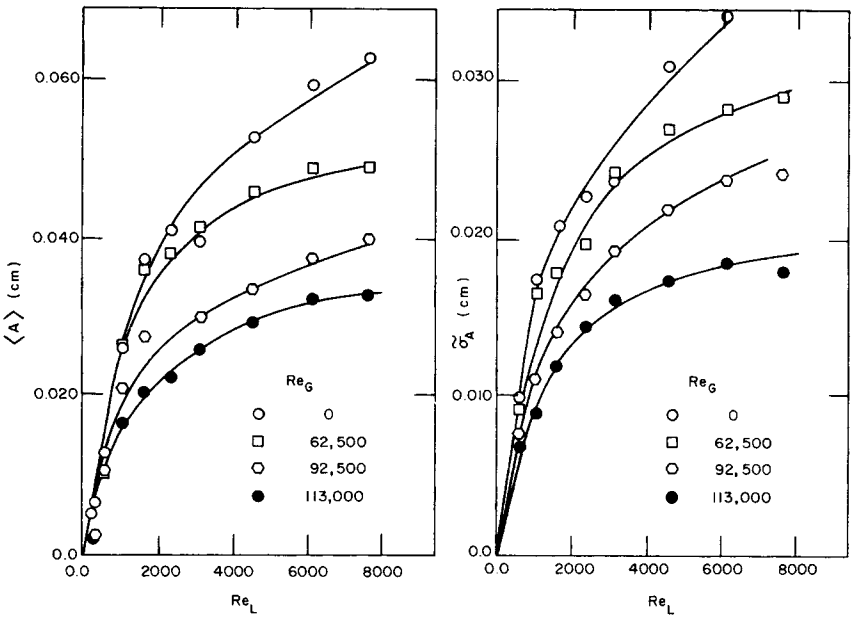

Fig. 10. Mean and standard deviation of large wave amplitude.

value of about 0.005 cm. If one compares this with the density distribution for the small waves on the substrate (Chu and Dukler, 1974), it is seen that even this smallest of large waves is about 3 times the size of the substrate waves.

As liquid flow rate increases ($Re_L \sim 1000$ to 3000), a second class of large waves with a modal amplitude of 0.030 to 0.034 cm appears. The continued existence of waves having 0.005-cm modal amplitude is still clearly evident. At $Re \simeq 3000$ a third type of large wave appears. These waves seem to be of about twice the amplitude of the second group, and this suggests they are formed by a process of coalescence of two waves each having amplitude of 0.030 to 0.034 cm. The existence of this process of coalescence has been well documented by Hewitt and Hall-Taylor (1970). At $Re = 6000$ and above, the intermediate wave size seems to have disappeared and the secondary wave size has a modal value of amplitude of about 0.064 cm. Data at still higher flow rates confirm this observation and indicate that the probability density tends to be increasing uniform with all wave sizes being observed on the surface.

The strongly bimodal distribution of amplitude is especially clear from Figure 9 where data at $Re_L = 1600$ is shown for a range of gas rates and interfacial shear. Again it is clear that even the large waves consist of two classes; one group which distributes in amplitude around a modal value of about 0.005 cm and a second group having modal values from 0.030 to 0.040 cm.

The existence of multiple peaks in the density distribution has not been evident from any earlier published data, and it is now easy to understand why past modeling efforts have been unproductive. Even the physical basis for the existence of these several classes of large wave sizes is not understood.

The mean value $<A>$ and the standard deviation $\tilde{\sigma}_A$ are given in Figure 10. These data show the expected increase with liquid flow rate and decrease with gas flow. Data were also taken on the statistics of h_{mn}. These data show that the standard deviation in the minimum film height at the base of the wave is very small. It is thus possible to conclude that the observed standard deviation

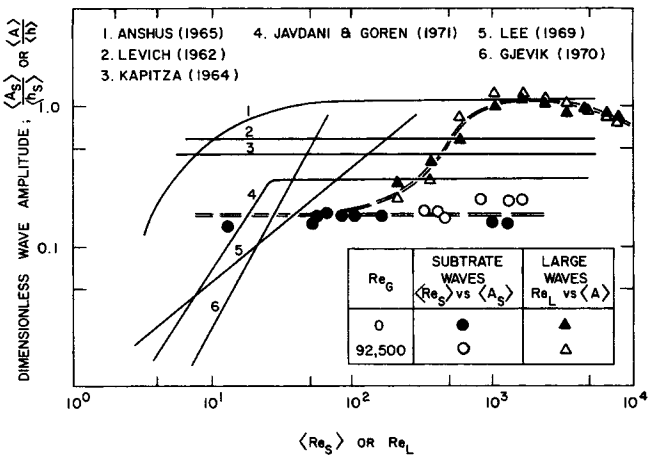

Fig. 11. Theory vs. experiment: wave amplitude.

in A results from randomness of values of the film thickness at the peak of the wave.

The dimensionless mean amplitude of large waves as defined by $<A>/<h>$ is compared with six theoretical predictions in Figure 11. Also shown for comparison are data for the waves on the substrate. The abscissa for these substrate data is the Reynolds number of the substrate. Above $Re_L \simeq 1000$ the Anshus (1965) theory shows reasonable agreement with data. However, it is clear that the trend of the data are in disagreement with the trend of any of these theories.

Wave Base T_b and Wave Separation Time T_s. The mean and standard deviation of the time base dimension T_b of the large waves appears in Figure 12. The frequency of the large waves, defined as $f = 1/<T_s>$ is shown in Figure 13 and the ratio of the front to the back dimension of the wave, T_{bf}/T_{bb}, appears in Figure 14. All of these time domain data suggest an important transition at a $Re_L \simeq 750$, and the observation is substantiated by other measurements such as covariance functions (Chu, 1973). Study of the amplitude probability density data (such as in Figure 9) suggests that the transition is associated with

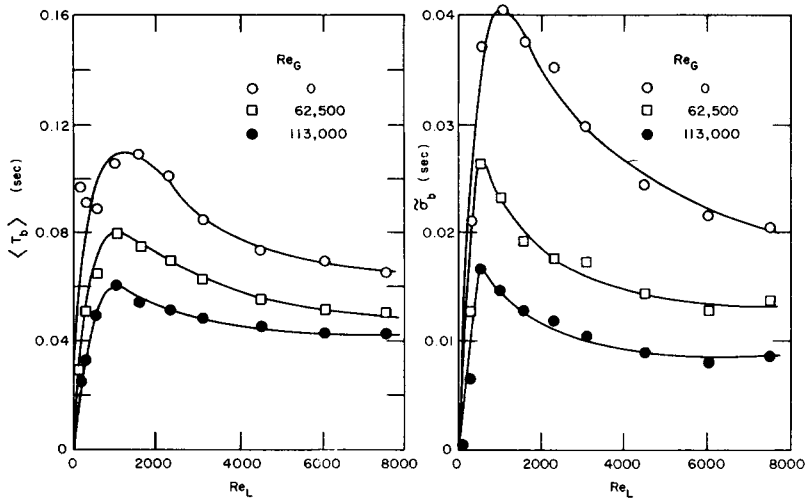

Fig. 12. Mean and standard deviation of base dimension of large waves.

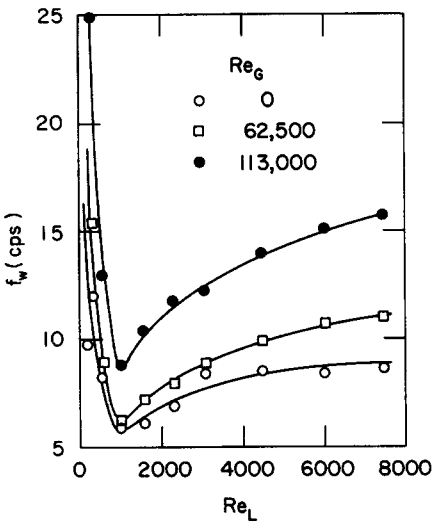

Fig. 13. Frequency of large waves.

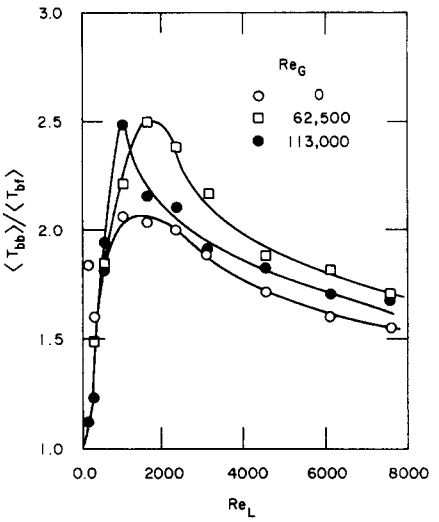

Fig. 14. Ratio of mean back to front dimension of large waves.

the appearance of a second characteristic wave size. At lower rates the amplitude density function is unimodal. At higher values it has several peaks.

Many theories have tried to predict the wave frequency and these attempts are compared with experiment of this study and Kapitza's data (1964) in Figure 15. For comparison, included on this graph are data for frequency of small waves on the substrate f_s vs. Reynolds number of the substrate flow $<Re_s>$. No theory adequately predicts the frequency of the large waves.

Typical probability densities of the wave base for the large waves at $Re_L = 1600$ are shown in Figure 16. Considering that we observe several characteristic wave amplitudes, the fact that all these waves have only one characteristic base time distribution seems remarkable. Because the wave velocity, time, and length are related, the densities for base length may look considerably different than for time of passage of the base. However, the physical principle which requires T_b to be narrowly distributed is not yet clear.

The measured probability densities for separation time are, on the other hand, consistent with the existence of several classes of waves. Figure 17 shows bimodal peaks for $Re_L = 1600$. Data for other rates are similarly consistent.

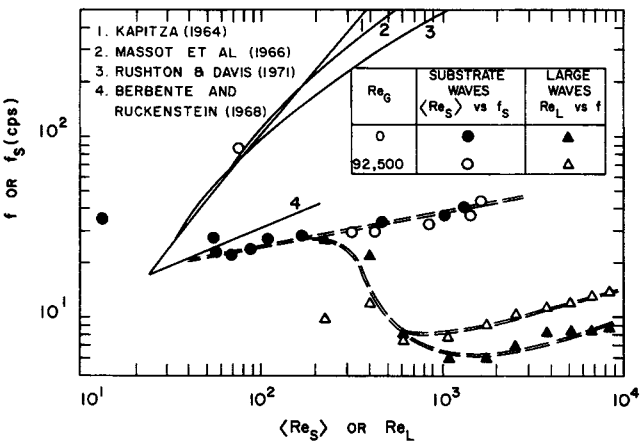

Fig. 15. Theory vs. experiment: wave frequency.

Wave Velocity and Wavelength. The velocity of the large waves c can be obtained either from the phase spectrum between time series measured at two stations with l distance apart,

$$\tilde{\theta}(f) = 2\pi f \frac{l}{c} \tag{12}$$

or from their cross-covariance function at

$$\tilde{C}_{12}\left(-\frac{l}{c}\right) \geq C_{12}(\tau) \quad \text{for all } \tau \tag{13}$$

Wave velocities determined for various gas and liquid flow rates using phase spectrum are given in Figure 18. These data show the expected trend of increasing velocity with both gas and liquid rate.

Theories which predict the wave velocity usually show that the ratio of the velocity to the mean film thickness depends on the Reynolds number. Figure 19 compares velocity based on the experimental data for large waves normalized by the velocity

$$\langle u \rangle = \frac{\nu}{4} \frac{Re_L}{\langle h \rangle} \tag{14}$$

with available theories. Included for comparison are the data on velocities of the small waves on the substrate. It is clear that the theories do not do an acceptable job of predicting the true situation.

The average wavelength of large waves is calculated from

$$\langle \lambda \rangle = c \langle T_s \rangle \tag{15}$$

The dimensionless wavelength

$$N_\lambda = \frac{\langle \lambda \rangle}{2\pi} \frac{g\rho}{g_c \sigma} \tag{16}$$

is plotted against the Weber number of the film

$$We = \frac{\langle u \rangle \langle h \rangle}{\sigma} \tag{17}$$

in Figure 20, where it is compared with the prediction of five theories. Data for small waves on substrate is also included. No theory is satisfactory.

The clue to the reason for the poor performance of all

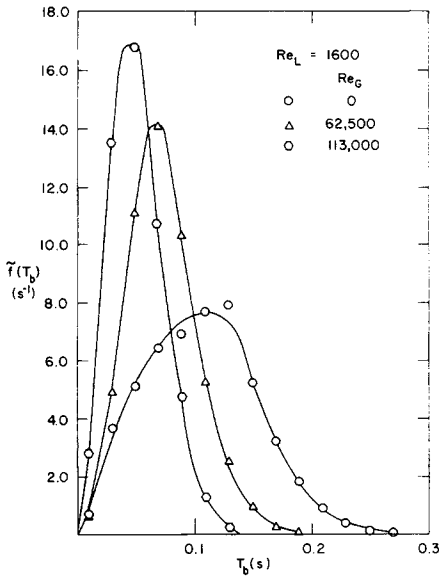

Fig. 16. Probability density of large wave base times.

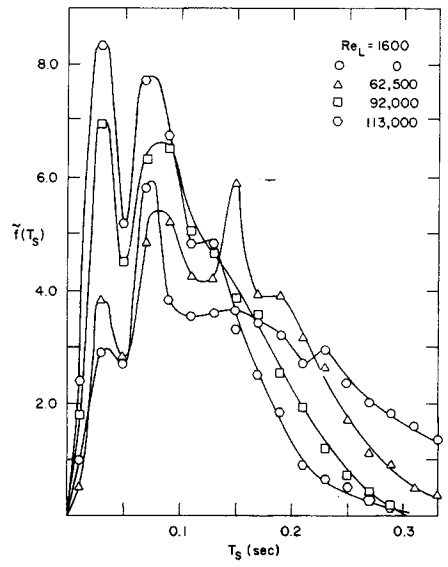

Fig. 17. Probability density of large wave separation time.

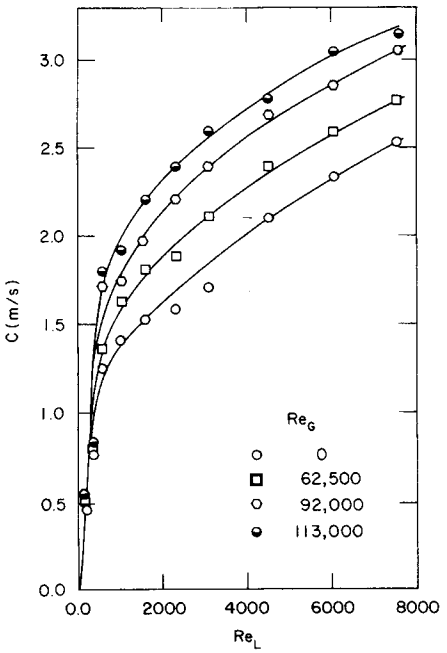

Fig. 18. Velocity of the large waves.

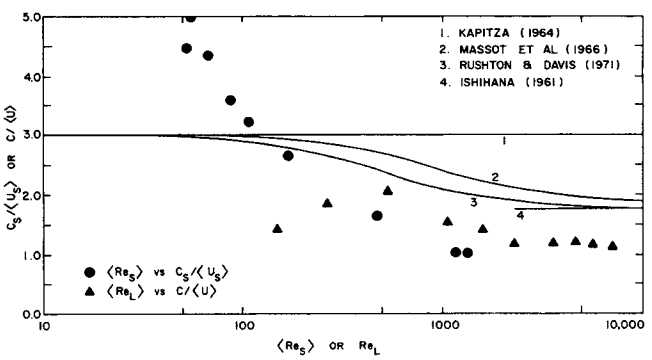

Fig. 19. Theory vs. experiment: wave velocity.

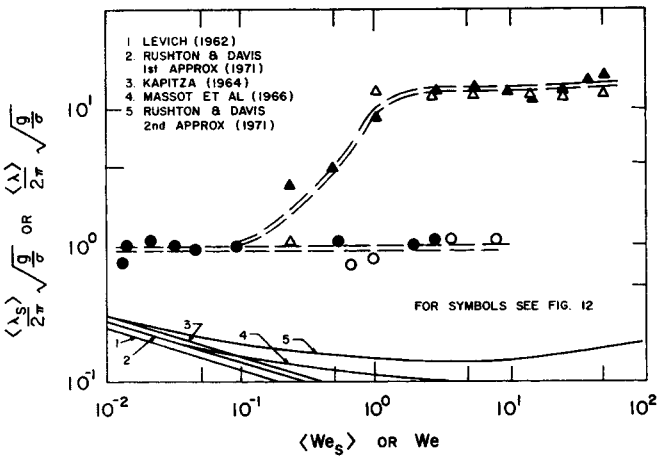

Fig. 20. Theory vs. experiment: wavelength.

these theories probably rests in Figure 14 where the data shows that the waves are strongly asymmetrical. All theories which have been published describe the wave profile with a few terms in a Fourier series expansion. Inclusion of additional terms makes the problem mathematically intractable. But in order to describe these large waves with the degree of asymmetry shown in Figure 14, 6 to 7 terms of a Fourier series is needed. As will be shown in the paper to follow, it is possible to use orthogonal expansions which can describe this shape with fewer terms.

Two Dimensionality of the Large Waves. Cross covariance function for film thickness were measured between probes located at 90 and 180° around the periphery of the tube at the same position along the tubes in the flow direction. These data (see Chu, 1973) clearly demonstrate that the large waves are two-dimensional rings even at substantial flow rates and interfacial shear.

CONTRIBUTION OF LARGE WAVES TO THE INTERFACIAL RESISTANCE FOR GAS FLOWS

Innumerable experimental measurements have demonstrated that pressure drop during gas flow over a wavy, annular liquid film in a pipe exceeds that for flows in liquid free pipes by multiples of 3 to 30 (see, for example, Hall-Taylor and Nedderman, 1968; Hewitt, 1969 and Dukler, 1972). Gazely (1949) conclusively demonstrated that in the absence of interfacial waves the gas phase shear is equivalent to that for flow over a solid surface. Thus, the increased resistance to flow is attributed to the presence of interfacial waves and a highly enhanced process of momentum transfer takes place as a result. A similar situation exists on the surface of the sea (Stewart, 1967) where the rate of growth of ocean waves depends on this process of momentum transfer. The sea surface consists of large gravity waves as well as small wavelets, and a controversy has existed for some time as to the relative contribution of the small and large waves to the wind-wave interactions. This is an important question to those attempting to model the process. Wu (1969, 1970) seems to have demonstrated from indirect evidence that separation around the small waves riding on top of the gravity waves supports the increased shear stresses observed in the wind. However, conclusive evidence has yet to be presented despite many studies reported from both laboratory and open sea measurements.

For film flow in pipes we have identified three characteristic waves; the large waves discussed in this paper, the small waves moving over the substrate (Chu and Dukler, 1974), and small waves riding on the larger waves (Chu, 1973). (It is likely that the small waves on the substrate and on the large waves differ only because the liquid depth differs.) It is important to identify which of these wave types cause the observed large shear stress and pressure drop in the gas phase so that competent models can be formulated to predict the two phase pressure drop and the transfer of heat and mass in the gas phase. Jameson (1971) has suggested that the large waves are dominant factors which control the total observed pressure drop.

Pressure fluctuations as well as pressure drop are substantially larger during two-phase annular flow than for flow of the gas alone (Telles, 1968). If increased pressure drop takes place in the gas phase due to the large waves, then when such a wave moves past a fixed pressure measuring station, a pressure fluctuation would be observed which should coincide with the fluctuations in film thickness due to these large waves. The fluctuations associated with the small waves are so small that much of this signal would be lost in the noise. Thus pressure and film thickness would be expected to correlate at frequencies characteristic of the large waves. In these experiments small pressure taps were located between each film thickness electrode pair as shown by Chu and Dukler (1974, Figure 3). Figure 21 shows typical experimental data for auto spectra of pressure and film thickness fluctuations about the mean and the cross spectra between the pressure and film thickness fluctuations. The auto spectra have been normalized by the second central moment and the cross spectra by the product of the square roots of the second moments for pressure and film thickness. These spectra have been processed to remove certain very narrow peaks which were shown to be due to low frequency vibration of the system. Comparing these

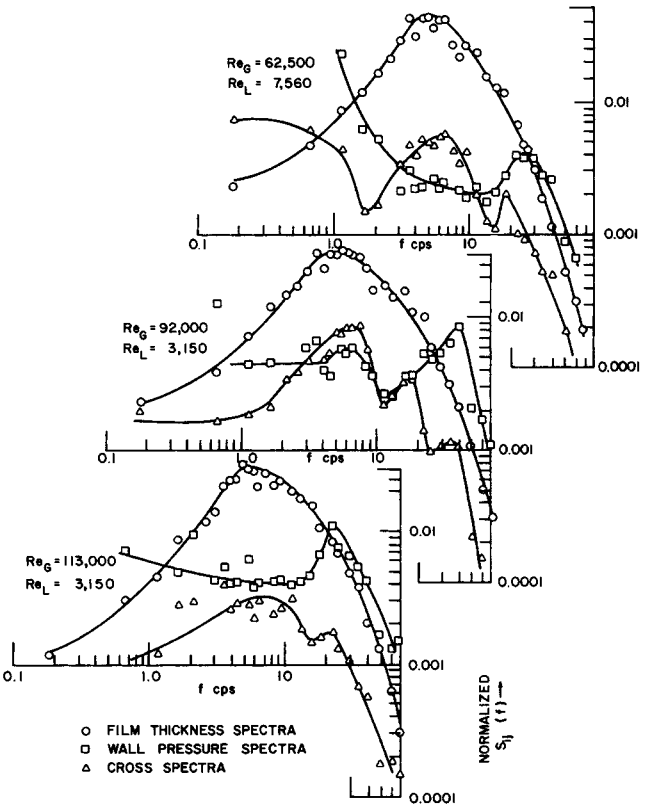

Fig. 21. Film thickness and pressure spectra.

curves shows only weak correspondence between pressure and film thickness but a strong correspondence between certain features of the cross and film thickness spectra. In particular, there exists a strong peak in the cross spectra corresponding to the main lobe of the film thickness spectra. This lobe has been shown earlier in the paper to correspond to the frequency of the large waves. Thus the existence of correlation in the region of the large waves is clear. Now it remains to determine the quantitative contribution of the large waves to the increased resistance for gas flow. With simultaneous records of pressure and film thickness, it is possible to extract information on the form drag of the large waves from the cross spectral density function. Such a direct determination of the form drag has never before been reported.

Let x be the coordinate axis in the direction of flow. The force exerted by the gas on the wave F_x, per unit area is

$$\frac{F_x(t)}{a_x} = \frac{1}{\lambda}\int_{\lambda/2}^{\lambda/2} P(x,h,t)\,\frac{dh(x,t)}{dt}\,dx \qquad (18)$$

where a_x is the wave area projected on the x-coordinate, λ is the wavelength, and $P(x,h,t)$ is surface pressure on the wave. From the above equation one can evaluate the time average form drag around the waves.

$$\tau_{FD} = \left\langle \frac{F_x(t)}{a_x} \right\rangle = \lim_{T\to\infty} \frac{1}{2T}\int_{-T}^{+T} \frac{1}{\lambda}\int_{-\lambda/2}^{+\lambda/2} P(x,h,t)\,\frac{dh(x,t)}{dt}\,dx\,dt \qquad (19)$$

Interchanging the integration order and assuming the waves are moving without changing shape at constant velocity c, the equation becomes

$$\tau_{FD} = -\frac{1}{c}\left\{ \lim_{T\to\infty} \frac{1}{2T}\int_{-T}^{+T} P(h,t)\,\frac{dh}{dt}\,dt \right\} \qquad (20)$$

If the simultaneous time series $P(h,t)$ and $dh(t)/dt$ are available, the above equation provides the required information on the form drag around the waves. However, the measured time series is $h(t)$ not its derivative and the process of differentiation can introduce large errors and is to be avoided. Let $\dot{h}(t) = dh(t)/dt$. The bracketed term in Equation (20) is the cross correlation between the two processes $\dot{h}(t)$ and $P(h,t)$ at zero time lag $\tilde{R}_{p\dot{h}}(0)$. If the stochastic processes $\hat{h}(t)$ is differentiable in the mean square sense and stationary, the following useful result exists (Papoulis, 1965):

$$\tilde{R}_{p\dot{h}}(0) = \frac{d}{d\tau}\tilde{R}_{ph}(0) \qquad (21)$$

Substitute Equation (21) into Equation (20), and expressing $\tilde{R}_{ph}$ as the Fourier transform of the cross spectrum yields

$$\tau_{FD} = -\frac{2\pi}{c}\int_{-\infty}^{+\infty} f\,\tilde{Q}_{ph}(f)\,df \qquad (22)$$

where $\tilde{Q}_{ph}(f)$ is quadrature spectrum of $\hat{P}(h,t)$ and $\hat{h}(t)$. Since the liquid film is so thin, it is plausible to assume that the wall pressure $\tilde{P}(0,t)$ is identical to the pressure on the wave surface $\hat{P}(h,t)$. Hence the form drag of the wave can be calculated from the quadrature cross spectrum between the wall pressure and film thickness [that is, the imaginary part of cross spectrum $\tilde{S}_{ij}(f)$]. Furthermore, the drag coefficient C_D can be estimated as follows:

$$C_D = \frac{2\langle\lambda\rangle\tau_{FD}}{\langle A\rangle\,\rho_G(U_G - c)^2} \qquad (23)$$

Table 2 presents values of the total interfacial shear τ_i as calculated from the pressure gradient in the gas phase

$$\tau_i = \frac{\Delta P}{\Delta L}\left[\frac{D - 2\langle A\rangle}{4}\right] \qquad (24)$$

and the shear due to the large waves τ_{FD} as calculated from equation (22). A comparison of these quantities shows that the resistance due to the large waves never exceeds 4% of the total measured resistance as expressed by the total interfacial shear. One thus is led to conclude that the primary contribution to the increased shear in annular flow is the small waves which exist on the interface. This result is identical with the conclusions reached by Wu (1970) for wind driven ocean waves.

Table 2. Interfacial Shear Stress Due to Large Waves

Re_G	Re_L	τ_i*	τ^*_{FD}	$100\,\frac{\tau_i}{\tau_{FD}}$	C_D
62,500	3,150	36.0	0.8	2.2	0.18
	4,130	47.1	1.2	2.6	0.26
	7,360	67.9	1.5	2.2	0.29
92,000	1,600	53.0	1.2	2.3	0.16
	3,150	72.6	2.1	2.9	0.23
	4,130	84.1	3.2	3.8	0.33
	7,360	119.1	3.8	3.2	0.36
113,000	1,600	87.0	1.7	1.9	0.20
	3,150	119.0	2.6	2.2	0.23
	4,130	131.1	3.4	2.6	0.25
	7,360	182.5	4.5	2.5	0.31

* τ expressed in dynes/cm².

ACKNOWLEDGMENT

The work was supported by a grant from the U.S. Department of Interior, Office of Saline Water.

NOTATION

A = wave amplitude of large waves
A_s = wave amplitude of small waves
a_x = projected wave area on x-coordinate
C = velocity of large waves
C_s = velocity of small waves
$\tilde{C}_{ij}$ = covariance function
C_D = drag coefficient
D = pipe diameter
F_x = force exerted by the gas on the wave
$\tilde{F}$ = probability distribution function
f = frequency in cps
f_m = modal frequency
f_w = frequency of large waves
f_s = frequency of small waves
$\tilde{f}$ = probability density function
g_c = conversion constant
g = acceleration of gravity

h = film thickness
h_s = substrate film thickness
h_{mx} = film thickness at the crest of the wave
h_{mn} = film thickness at the trough in the front of the wave
h'_{mn} = film thickness at the trough in back of the wave
$\dot{h}$ = time derivation of film thickness
l = separation distance between probes
N_λ = dimensionless wavelength
P = pressure
$\Delta P/\Delta L$ = pressure gradient
$\tilde{Q}$ = quadrature-spectrum
Re_L = input liquid Reynolds number
Re_S = substrate Reynolds number
Re_G = input gas Reynolds number
$\tilde{S}_{ij}$ = spectrum function
$\tilde{S}_{eq}$ = equilibrium spectrum
T = wave period
T_b = time for passage of base of wave
T_{bf} = time for passage of front of wave
T_{bb} = time for passage of the back of the wave
T_s = wave separation time
t = time
u = velocity in x direction
u_s = substrate velocity in x direction
u_G = average gas velocity in x direction
We = Weber number of large wave
We_s = Weber number of small wave
x = coordinate direction

Greek Letters

γ = kinematic surface tension
$\tilde{\theta}$ = phase spectrum
λ = wave length
μ = viscosity
$\tilde{\mu}$ = ith central moment
ν = kinematic viscosity
ρ = liquid density
ρ_G = gas density
σ = surface tension
$\tilde{\sigma}_A$ = standard deviation of wave amplitude
$\tilde{\sigma}_b$ = standard deviation of wave base
τ = time lag
τ_i = interface shear
τ_{FD} = form drag
$<>$ = expected value
$\wedge$ = random variable

LITERATURE CITED

Alves, G. E., "Cocurrent Gas Liquid Pipeline Contactors," *Chem. Eng. Progr.*, **66**(7), 60 (1970).

Anshus, B. E., "Finite Amplitude Wavy Flow on a Thin Film on a Vertical Wall," Ph.D. dissertation, Univ. of Calif., Berkeley (1965).

Berbente, C. P., and E. Ruckenstein, "Hydrodynamics of Wavy Flow," *AIChE J.*, **14**, 774 (1968).

Burling, R. W., "The Spectrum of Waves at Short Fetches," *Dentschen Hydrogr. Zeitschrift*, **12**, 45 (1959).

Chu, K. J., "Statistical Characterization and Modelling of Wavy Liquid Film in Vertical Two-phase Flow," Ph.D. dissertation, Univ. Houston, Texas (1973).

———., and A. E. Dukler, "Statistical Characteristics of Thin, Wavy Films: II. Studies of the Substrate and its Wave Structure," *AIChE J.*, **20**, 695 (1974).

Cichy, P. T., J. S. Ultman, and T. W. F. Russell, "Two-phase Reactor Design: Tubular Reactors," *Ind. Eng. Chem.*, **61**, 6 (1969).

Dukler, A. E., "Characterization, Effects and Modelling of the Wavy Gas-Liquid Interface," in *Progress in Heat and Mass Transfer*, Pergamon, New York (1972).

Gazely, C. A., "Interfacial Shear and Stability in Two Phase Flow," Ph.D. dissertation, Univ. Delaware, Newark (1949).

Gjevik, B., "Occurrence of Finite-Amplitude Surface Waves on Falling Liquid Film," *Phys. Fluids*, **13**, 1918 (1970).

Guerreri, G., and C. J. King, "Design Falling Film Absorbers," *Hydrocarbon Processing*, 131 (1974).

Hall-Taylor, N. S., and R. M. Nedderman, "The Coalescence of Disturbance Waves in Annular Two-phase Flow," *Chem. Eng. Sci.*, **23**, 551 (1968).

Hess, G. D., G. M. Hildy, and E. J. Plate, "Comparison Between Wind Waves at Sea and in the Laboratory," *J. Marine Res.*, **27**, 216 (1969).

Hewitt, G. F., "Disturbance Waves and Annular Two Phase Flow," Symp. Fluid Mechanics and Measurement in Two Phase Systems, Leeds, England (1969).

———., and N. S. Hall-Taylor, *Annular Two-phase Flow*, Pergamon Press, New York (1970).

Hicks, B. L., "Estimation of the Spectrum Function for Small Wind Wave," in *Ocean Wave Spectra*, Prentice-Hall, Englewood Cliffs, N. J. (1963).

Ishihara, T., Y. Iwagak, and Y. Iwasa, "Discussion on Roll Waves and Slug Flows in Inclined Open Channels," by Paul Mayes, *Trans. Am. Soc. Civil Eng.*, **126**, 548 (1961).

Jameson, G. J., "The Contribution of Disturbance Waves to the Overall Pressure Drop in Annular Two Phase Flow," *Trans. Inst. Chem. Eng. (London)*, **49**, 42 (1971).

Javdani, K., and S. L. Goren, "Finite-Amplitude Wavy Flow on Thin Film," in *Progress in Heat and Mass Transfer*, Pergamon, New York (1972).

Kapitza, P. L., "Wave Flow of Thin Layers of a Viscous Fluid," in *Collected papers of P. L. Kapitza*, MacMillan, New York (1964).

Kinsman, B., "Surface Waves at Short Fetches and Low Wind Speeds—a Field Study," Chesapeake Bay Inst., Tech. Rep. XIX Ref 60-1, 581 (1960).

Lee, J., "Kapitza's Method of Film Flow Description," *Chem. Eng. Sci.*, **24**, 1309 (1969).

Levich, V. G., *Physiochemical Hydrodynamics*," pp. 674-692, Prentice-Hall, Englewood Cliffs, N. J. (1962).

Mossot, C., F. Irani, and E. N. Lightfoot, "Modified Description of Wave Motion in Falling Film," *AIChE J.*, **12**, 445 (1966).

Papoulis, A., *Probability, Random Variable and Stochastic Process*, McGraw-Hill, New York (1965).

Phillips, O. M., "The Equilibrium Range in the Spectrum of Wind-Generated Waves," *J. Fluid Mech.*, **4**, 426 (1958).

Poshniak, D. W., "An Investigation of the Interfacial Disturbances in Vertical Two-phase Flow," Ph.D. dissertation, Univ. Washington, Seattle (1969).

Rushton, E., and Q. A. Davis, "Linear Analysis of Liquid Film Flow," *AIChE J.*, **17**, 671 (1971).

Sack, M., "Falling Film Shell-and-Tube-Exchangers," *Chem. Eng. Progr.*, **63**, 55 July (1967).

Stewart, R. H., "Laboratory Studies of the Velocity Field Over Deep-Water Waves," *J. Fluid Mech.*, **42**, 733 (1970).

Telles, A. S., "Liquid Film Characteristics in Vertical Two-phase Flow," Ph.D. dissertation, Univ. Houston, Texas (1968).

———., and A. E. Dukler, "Statistical Characteristics of Thin, Vertical Wavy Liquid Films," *Ind. Eng. Chem. Fundamentals*, **9**, 412 (1970).

Webb, D., "Two-phase Flow Phenomena," Ph.D. dissertation, Univ. Cambridge, England (1970).

Wicks, M., "Liquid Film Structure and Drop Size Distribution in Two-phase Flow," Ph.D. dissertation, Univ. Houston, Texas (1967).

Wu, J., "A Criterion for Determining Air-Flow Separation From Wind Waves," *Telles*, **21**, 707 (1969).

———., "Wind-Wave Interactions," *Phys. Fluid*, **13**, 1926 (1970).

Manuscript received December 2, 1974; revision received and accepted February 3, 1975.